COMPUTATIONS OF THREE–DIMENSIONAL DEFORMATIONS OF HEXAGONAL DUCTS COMPARED WITH EXPERIMENTAL RESULTS

J.E. ASH, A.H. MARCHERTAS

Reactor Analysis and Safety Division,
Argonne National Laboratory, Argonne, Illinois 60439, U.S.A.

SUMMARY

The liquid metal fast breeder reactor (LMFBR) core structure consists of a matrix of hexagonal subassembly ducts. Safety considerations require that the deformation response of the hexagonal ducts to a postulated local energy release be predictable. Deformation of the structural matrix can interfere with control-rod withdrawal and can cause local reduction in coolant flow passages. For example, a fuel pin cladding failure resulting in fission gas release will create a pressure-pulse loading on the internal walls of a subassembly hexcan duct. This pressure pulse will attenuate as it travels towards the ends of the hexcan with the result that a three-dimensional, transient pressure loading is exerted. A three-dimensional, finite-element structural code SADCAT (Structural Analysis for 3-Dimensional Core Assembly Transient) has been developed to compute the hexcan response to such loadings. Computations made with the SADCAT code have been compared with experiments performed for simulated EBR-II and FFTF out-of-pile ducts. Comparisons are also made with computed two-dimensional code results.

The dynamic response of an EBR-II hexcan to a fuel pin failure was simulated experimentally by gas-pressurizing a centrally located tube to the bursting point. The hexcan test rig was immersed in water. The gas escaping from the tube rupture created a pressurized bubble in the surrounding liquid, and under the action of the internal loading the walls of the hexcan deformed. The resulting pressure, strain, and deflection data were recorded. The gas discharge from the rupture is described in an analytical model, the corresponding bubble formation and pressure-pulse distribution within the hexcan subassembly are computed with an implicit hydrodynamics code called ICECO (Implicit Continuous Eulerian Code). The resulting computed pressure distribution provides the input to the SADCAT computation for the dynamic response of the hexcan. Good correlations were obtained between the experimental data for the measured pressures and final permanent hexcan deformations and the computed results.

An FFTF out-of-pile hexcan was slowly pressurized to failure and the deformation response as a function of pressurization was measured. These deflection data were compared with the three-dimensional code computations. The bending effects of the end constraints are found to extend an axial distance no greater than one equivalent-diameter for moderate loadings so that the hexcan deformation is uniform except for these end regions. For plastic deformations under higher loadings, the end effects will extend over a considerably greater distance, increasing with the deflection magnitude. For the region of uniform deformation, the problem reduces to a two-dimensional one, and constraining the axial deflection at the ends results in a plane-strain case. Within the elastic range, computations by a two-dimensional code STRAW, with suitably modified elastic moduli to account for the stiffening effect of the end constraints, compared well with the full three-dimensional SADCAT computations. For the larger plastic flow deflections, the plane-strain modifications in the plastic material properties led to some discrepancy in the results computed with the STRAW code. Throughout both the elastic and plastic deformation ranges, the deflection response is sensitive to the stress-strain material properties.

1. Introduction

The structural members of a reactor core consist largely of plate/shell-type components. The response of these members to hypothetical high-pressure loadings is of concern to reactor safety analysis. As a tool for design studies of structural integrity under postulated accident conditions, it is convenient to have an efficient structural-analysis computer code that can quickly and economically run through computations over a range of conditions. In many instances, a two-dimensional code is sufficient to determine maximum deformations and to predict, at least qualitatively, the general response behavior. However, under some hypothetical conditions, highly transient, sharply peaked local pressures can conceivably arise which will produce definite three-dimensional deformation. It is desirable in these cases to have available a three-dimensional structural code. Such a code would be useful also to determine, by means of comparisons, the extent to which the more simple (and economical) two-dimensional formulation can approximate the response. For these purposes, a three-dimensional code called SADCAT [1], and a similar two-dimensional version, STRAW [2], have been developed. An application of these codes will be presented in which the response of hexagonal subassembly fuel wrappers to internal pressures is predicted. Comparisons are made between computations and experimental results.

Other general-purpose finite-element structural codes exist, but employ implicit numerical-integration methods. Implicit methods have the advantage of being inherently stable, but a three-dimensional problem will generally require very large computer-storage and long running times. This disadvantage arises because the entire system of equations must be solved simultaneously at each time step. To reduce the computational demands, SADCAT and STRAW are formulated to solve explicitly the equations at only one point at a time. By this procedure the computer-storage requirement at each time step is grossly reduced. However, the explicit scheme can become unstable unless the time step is suitably small. Very small time steps may require many repetitive computations, but for the type of problem under consideration, a relatively small time increment is required for reasons other than stability. Thus, for reactor-accident problems, there may be a definite economic advantage in using an explicit code. The reasons for a small time step are (1) to obtain adequate resolution of the sharply varying pressure-pulse loading and (2) to follow closely the path-dependent stress-strain relationship, particularly for stress concentrations in the hexcan corners. These stress concentrations give rise to large local nonlinear inelastic strains.

Good correlations were found between the computed hexcan response and test data for simulated EBR-II fuel-pin-failure experiments. Comparisons are also presented for experiments performed with larger hexcans of the type contemplated for the FFTF reactor configuration.

2. The Three-dimensional Structural Dynamics Code

A general purpose code, SADCAT, has been developed for transient analysis of plate and shell structures. This code uses a lumped-mass system and an explicit time-integration procedure. In addition, it treats large displacements and elastic-plastic behavior of material. The code, therefore, is especially suited for structures subjected to high loading rates and undergoing large displacements.

The formulation within the code is based on the finite-element procedure, in which the discrete model of the structure consists of an assembledge of flat, triangular plate elements interconnected by nodes. Each element is associated with a convected coordinate system which is attached to the element. Thus, the convected coordinate system moves with the element and approximates the rigid-body motion of the element. In addition, each node is associated with a set of body coordinates which rotate with the node and coincide with the principal axes of the mass moment of inertia of the node.

The lumped masses and rotational inertias of the nodes are obtained as follows: The mass and moment of inertia of each element are calculated and then subdivided into three equal parts, each associated with the respective nodes of the element. This procedure is applied to every element so that the final mass and moments of inertia at each node consist of contributions from all adjacent elements. The principal moments of inertia are then determined at each node; the associated principal directions constitute the initial body coordinates. At the boundary the moments of inertia are made isotropic and the body coordinates are prescribed so that any required rotation can be imposed.

The total displacement of the element is decomposed into a rigid-body motion and a deformation. The rigid-body motion is defined by the motion of the convected coordinate system; the deformation is the displacement relative to the convected coordinates. Rotations of the nodal coordinates are described by Euler angles; the nodal coordinate components are updated at every time step.

The plate element is assumed to have linear in-plane displacements and cubic transverse displacements. The deformation displacements are computed from the relative displacements and relative rotations of the nodes. Following Argyris [3], the in-plane deformations are determined by side elongations of the element. The nonconforming shape functions developed by Bazeley [4], determine the flexural component of deformation. The strains are computed in the convected coordinate system: the first derivative of the in-plane displacement provides the membrane component of strain, and the second derivative (curvature) of the shape function yields the flexural component of strain.

The tensile data of true stress vs engineering strain are approximated by a multilinear curve with isotropic strain hardening. Yielding in the biaxial state of stress is handled by the von Mises yield criterion and a flow rule is assumed in the plastic regime. The plastic components of stress are evaluated by an algorithm introduced by Hartzmann and Hutchinson [5].

Internal nodal forces and moments are derived using a five-point trapezoidal integration across the element thickness and a three-point integration over the element plane. The transverse nodal forces are obtained from the requirement that the nodal forces of an element must be self-equilibrated.

In some problems in which the residual membrane forces are large and no external loads are present there is a tendency for certain nodes to oscillate in a snap-through mode. This effect is eliminated by a membrane artificial viscosity which can be specified as a percentage of critical damping.

The code accepts pressure-time histories, initial velocities, and displacements as external loads. With the mass, moments of inertia, and the external and internal forces known, the equations of motion are applied at the nodes. The equations of motion are integrated in time using the Newmark-β method [6]. Since the formulation is based on an explicit integration, the length of the prescribed time step is limited by a stability criterion. The code operation has been found to be quite efficient, taking about 2 msec/time-step/element on an IBM 370/195 computer.

3. Dynamic Experiments for EBR-II Hexcans

3.1 Description of the Experiments

Three-dimensional effects have been demonstrated in a series of tests performed by Koenig [7], at Argonne National Laboratory with out-of-pile EBR-II subassembly hexcans. In these tests, the response of a hexcan to the sudden pressure pulse created by a fuel-pin failure was measured. To simulate the pin cladding failure a single tube was pressurized with helium and predefected to burst at about 2000 psi. The defect was located so that the resulting pressure pulse created by the escaping gas was centered in the hexcan. The test rig, shown in fig. 1, was submerged in a drum of water.

3.2 The Pressure Loading within the Hexcan

To maximize the pressure pulse for a given tube pressure, a 1-in. slot was milled into the tube wall to insure the largest possible rupture opening. Typical ruptured tubes are shown in fig. 2. Immediately following rupture, the tube pressure fell to about 10% of the peak within 1.6 msec. The pressure in the bubble built up by the escaping gas reached a maximum of 350 psi, and sustained a wall-loading pressure above 100 psi for 2.3 msec. Tests at other burst pressures were performed, but a fairly constant ratio of 17% was found to hold between the maximum bubble pressure and the peak tube pressurization.

Irregularities in the shape of the rupture opening, as shown in fig. 2, raise questions about the effect upon the discharge rate of the gas, and possible unpredictable variations in the resulting pressure loading with corresponding lack of symmetry and reproducibility. To assure uniformity and establish reproducibility over a series of tests, the tube rupture was replaced by the symmetrical arrangement of orifices shown in fig. 3. Under these controlled conditions of the pressure source, the pulse peak was more sharply defined than for the tube-burst tests, and the decay of the bubble pressure was more uniform. We see in fig. 4 that for the tube rupture two pressure peaks appeared followed by an irregular decay. This indicates that the rupture did not reach its final size instantaneously, but progressed in at least two distinct stages. The first pressure peak corresponds to the initial breaking, and then in spite of the diminishing pressure ratio, the gas discharge is sustained by further widening of the opening. As a result, the bubble pressure peaks a second time before trailing off.

The maximum pressure was over the hexcan wall area midway between the ends of the 32-in. test length and opposite the gas-discharge source. The pressure loading attenuated as the pulse traveled towards the ends of the hexcan. Measurements of the decreasing pressure correlated with pressure computations made with a finite-difference hydrodynamic code ICECO [8]. For the test series in which the pressure variation along the length of the can was measured, the hexcan wall deformations were kept small. For later tests in which significant wall deformation occurred, the pressure distribution was not measured along the length of the hexcan, but was computed with the previously verified ICECO code.

The growth of the bubble computed with the ICECO code is shown in fig. 5. The computed bubble volume and mass transfer determine the density, and, assuming an isentropic expansion, the bubble pressure downstream of the orifice is determined. Computed pressure traces for the plenum and gas bubble are shown in fig. 6. The computed plenum pressure was verified by measurements of pressures in the gas-supply line. The bubble pressure is equal to the pressure exerted against the wall, and computed and measured values are compared in fig. 7.

3.4 The Hexcan Deformation and Comparison with Experiments

As the pressure pulse propagates from the midlength to the ends of the test hexcan, a pressure-time trace is generated at each fixed position along the axial length. Computed pressure traces at a sequence of such stations are shown in fig. 8. The peak of each trace diminishes with distance from the source. The problem of computing the hexcan deformation response is clearly three dimensional: the loading varies in the axial direction, and the hexcan geometry varies in the circumferential and radial directions. Hence, a three-dimensional structural code such as SADCAT is needed to compute the dynamic response of the hexcan. Computed deflection histories at stations along the hexcan length are shown in fig. 9.

A "periodic axisymmetry" was assumed for the computation in the sense that the same pressure loading was exerted against each of the six faces; consequently, the response was identical for all the faces. Actually, in the experiment, as shown in fig. 10, the deflections were not identical for each pair of diametrally opposed flats.

Since pressure measurements taken about the periphery demonstrated that a fairly uniform axisymmetric pressure loading was established at the wall, it appears that the deflection differences are due to a type of structural instability. A likely explanation is that the material properties, particularly as influenced by cold working, vary to a certain extent from corner to corner. The yield stress is highly sensitive to such variations, and yielding will occur in one corner, say, before occurring in the others. As a result, a plastic hinge will develop at this corner. Consequently, because of the abrupt change of slope in the stress-strain curve at the yield point, the local deformation rate will increase sharply, and the subsequent motion will distort the symmetry of the hexagonal shape.

In the computation, each face is assumed to have the same lengthwise deflection profile. For the comparison in fig. 11, the deflections of the three pairs of diametrally opposed flats are represented by an equivalent mean-volume expansion. Since the pressure source was located midway between the upper and lower ends of the hexcan, the upper half was assumed to be the mirror image of the lower half. Actually, in the experiment this symmetry was not maintained after the pressure pulses reached the open ends of the can. At the upper end, when the pressure pulse reaches the free surface of the water, a rarefaction wave is reflected back down the test can. However, when the primary pressure pulse leaves the lower end, it travels to the bottom of the containment tank and reflects as a compression wave. The net effect is that the lower half of the hexcan is exposed to greater pressure loading than the upper half. As a result, a slightly greater bulging of the lower half of the experimental duct is observed in fig. 11.

4. Quasi-Static Experiments for FFTF-Type Hexcans

4.1 Description of the Experiments

The hexagonal subassembly ducts for the EBR-II reactor core are considerably smaller than similar ducts currently contemplated for the FFTF-type cores. To study the response of larger subassembly ducts an out-of-pile test program is underway at Stanford Research Institute. The distance across flats for the test ducts is 4.5 in. compared to 2.25 in. for the EBR-II duct, and the wall thickness is increased to 0.120 in. from 0.040 in. To maintain essentially two-dimensional loading for code comparisons in preliminary dynamic tests, a line pressure-source was employed rather than a point source. The line source was along the axis and extended the length of the test duct. The resulting dynamic loading became essentially uniform in the axial direction.

Prior to the dynamic loading tests, sample hexcans were slowly pressurized until failure. The purpose of these preliminary tests was to study the effects of material properties and end conditions upon the hexcan response. It was found that for moderate deflections under hydrostatic loading, the central sections away from the ends deformed uniformly in the axial direction. Consequently, it can be assumed that for the central test section, two-dimensional conditions prevail, permitting the application of a two-dimensional code such as STRAW.

Two sample test hexcans are shown in fig. 12 after being slowly pressurized until failure. Both cans are type 316 stainless steel. However, the steel for the can on the left had been work-hardened by the final fabrication drawing process (corresponding to a nominal 20% cold working, with greater residual hardness in the corners). The can on the right had been annealed and was considerably more ductile. The central portion of the annealed can has expanded out to a circular shape (see fig. 13). The permanent diametral increase from midflat to midflat was nearly 1-in. (0.45-in. radial deflection). The can sustained an internal hydrostatic pressure in excess of 3000 psi before splitting at the corner. The can on the left was markedly less ductile. The corner fractured at a pressure of about 2500 psi; the maximum midflat diametral increase was only about 0.3-in.

4.2 Comparisons of Three-Dimensional with Two-Dimensional Computations and Experiments

The response of the hexcan to uniform internal pressurization was computed with both the two-dimensional STRAW code and the three-dimensional SADCAT code. The computed deflections were compared with deflections measured in the experiments. Attention is focused upon the annealed hexcan for comparisons with the experimental data. The STRAW code was applied to the uniformly loaded central portion of the hydrostatically pressurized test can. The stress-strain curve was adjusted for plane-strain conditions by a very simple method [9]. The Young's modulus was increased by the factor $1/(1 - \nu^2)$ and the yield stress by the factor $1/\sqrt{1 - \nu + \nu^2}$, where ν is Poisson's ratio. The adjustment for the plastic region consisted of increasing the slope of the stress-strain curve by the factor 4/3.

The plane-strain computation of the STRAW code advanced forward in time by finite-difference time steps Δt as the hexcan was slowly pressurized. The strains were expressed as total elongation divided by the original length, i.e., engineering strains. However, as the hexcan expanded, the wall thickness diminished, and the elemental stress forces were expressed as a stress multiplied by the actual instantaneous cross-section area, i.e., the true stress was used.

The sensitivity of the hexcan deflection to changes in material properties is indicated in fig. 14. The elastic properties and yield point were held fixed, but in the plastic range the stress was raised and lowered by fixed percentages. We see that lowering the plastic stress has a greater influence upon the deflection than raising the stress. The sensitivity of the deflection response to changes in the stress-strain relationship increases as the pressure is raised. At 3000 psi, a 10% reduction in the stress (corresponding to the given strain) caused the deflection to increase 30%.

4.3 The Three-dimensional Computations

In the hydrostatic tests the hexcan was slowly pressurized. The two-dimensional STRAW code was used to compute the midflat deflection at the section midway between the test duct ends. It was found, by comparison with longer lengths, that a 1-ft length was sufficient for the midflat deflection to be independent of the radial constraints imposed by heavy flanges at the ends. Unlike the radial constraints, axial constraints at the ends will stiffen the entire can against expansion. The stiffening effect is independent of the can length. At the end region the (lengthwise) deflection profile is nonuniform and computations for this region require a three-dimensional code. The boundary condition imposed by the end flange constrains the slope as well as the displacement, i.e., the flange imposed a bending moment at the end as well as a radial force component. For the prescribed end conditions of zero slope and radial displacement, the deflection profiles shown in fig. 15 were computed with SADCAT. The bending moment induced an inflection point and a slight bulging appeared near the end. The maximum deflection occurred at the bulge rather than at the midsection as might otherwise be expected. This bulging phenomenon has been previously described [10] for thin circular tubes. The bulge produced an additional deflection of about 10% above the uniform deflection at the sections more remote from the ends. The stiffening effect of the axial constraint is shown in fig. 15. The computation indicates, for example, that at an internal pressurization of 2000 psi, the deflection is reduced 20 mils, or 10% less than would occur if the duct were permitted to contract freely in the axial (lengthwise) direction.

The dynamic effects of the loading rate were computed with the three-dimensional SADCAT code. Midflat deflections for loading rates of 250, 1000, and 2000 psi/msec are compared in fig. 16. Also shown in the figure, for reference, are the experimental deflections for hydrostatic loading. At the highest loading rate of 2000 psi/msec, a strong inertial lag occurred during the intial response. The deflection quickly accelerated and overshot the hydrostatic magnitude by about 33% at a pressure of 1200 psi. When the loading rate was slowed to half the value (i.e., 1000 psi/msec), the overshoot was significantly reduced. If the pressurization were stopped at 1200 psi, say, the final permanent deflection would be 180 mil for the slower loading rate compared to about 230 mil for the higher rate. It is difficult, however, to generalize about the effect of loading rates upon the final permanent deformation. We see, for example, in fig. 16 that although the higher loading rate significantly increased the final deformation at 1200 psi, at the higher internal pressure of 2000 psi the loading rate had a negligible influence.

Variations in loading rates at higher pressures (beyond 1700 psi in fig. 16) had little influence upon the final permanent deformation. In contrast, at smaller pressures the rate had a strong influence upon deflections. This contrasting behavior is explained by the fact that, at the lower pressures, the dominant deflection mode of the hexcan face is that of a bending plate. At the higher pressures the duct has expanded out to a circular cylinder shape (see fig. 13). For the plate deflection mode much of the material (with the exception of the corners) is yet in the elastic range and the dynamic oscillatory response effects are not so quickly damped out. In the cylindrical deflection mode, however, the plastic-material zone is uniformly (axisymmetrically) distributed, and the inertial dynamic effects are quickly absorbed and suppressed.

The effect of axially constraining the hexcan is shown in fig. 17 for the loading rate of 400 psi/msec. There was little influence at the smaller pressures, but at the higher pressures above 1300 psi expansion caused the can to contract in length. At the 3000 psi internal pressure, the 1-ft length was reduced by more than 0.6 in. The elements underwent a large compressive strain in the axial direction and consequently strained more easily in the circumferential direction. As a result, the expansion of the duct was much greater when the ends were free to contract than for constrained ends. At 3000 psi, freeing the ends increased the maximum (midflat) deflection by 27%, from 300 to 380 mils.

Conclusions

In general, an accidental pressure loading exerted against the walls of a fuel-pin hexagonal subassembly wrapper can be expected to be three-dimensional. Computations performed with a three-dimensional code, SADCAT, of the final permanent deflection profile of an out-of-pile EBR-II test hexcan correlated well with the experimental data. The experiment simulated a fuel-pin failure by pressurizing a centrally located tube to the bursting point. The discharge gas bubble created a pressure-pulse loading on the walls of the hexcan. Since the pressure load varied (by attenuation) along the length of the hexcan, three-dimensional deformations resulted.

Further tests have been performed for larger hexcans of the type that may be used in the FFTF reactor. For slow pressurization, the internal wall loading was uniform over the length of the hexcan duct. Midflat deflections over the region midway between the duct ends correlated well with computations performed with the two-dimensional version of the code. The correlation remained good for relatively large deflections involving strains in excess of 20%. The full three-dimensional code was required to compute the deflection profile in the end regions.

It appears that when the stress-strain properties are suitably modified for plane-strain conditions, the two-dimensional code can predict the maximum deflection occurring opposite a centrally located pressure source. To compute the full deflection profile, a three-dimensional code appears to be required. Computations with the three-dimensional code demonstrated that an increased dynamic loading rate can significantly increase the final permanent deformation. Also, rather small variations in the material properties can result in rather large variations in the final permanent deflection.

References

[1] MARCHERTAS, A. H., BELYTSCHKO, T. B., "Nonlinear Finite-Element Formulation for Transient Analysis of Three-Dimensional Thin Structures," ANL-8104 (June 1974).

[2] KENNEDY, J. M., "Nonlinear Dynamic Response of Reactor Core Subassemblies," ANL-8065 (January, 1974).

[3] ARGYRIS, J. H., KELSEY, S., KAMEL, H., "Matrix Methods of Structural-Analysis: A Precis of Recent Developments," Matrix Methods of Structural Analysis, ed. by B. F. deVenbeke, AGARDOgraph 72, Pergamon Press, (1964).

[4] BAZELEY, G. P., CHEUNG, Y. K., IRONS, B. M., ZIENKIEWICA, O. C., "Triangular Elements in Bending-Conforming and Nonconforming Solutions," Proceedings of the Conference on Matrix Methods in Structural Analysis, Wright-Patterson Air Force Base, Ohio (1965).

[5] HARTZMAN, M., HUTCHINSON, J. R., "Nonlinear Dynamics of Solids by the Finite Element Method," Computers and Structures, Vol. 2, 47-77 (1972).

[6] NEWMARK, N., "A Method of Computation for Structural Dynamics," Journal Eng. Mech., Div. A.S.C.E., 67-94 (1959).

[7] KOENIG, J. F., et al, "Response of an EBR-II Hexagonal Can to a Limited Release of High-Pressure Gas," Trans. Am. Nucl. Soc., 14, p. 286 (1971).

[8] WANG, C. Y., CHANG, Y. W., and FISTEDIS, S. H., "Application of Implicit Continuous Eulerian Containment Code to Low-Energy Excursions," Trans. Am. Nucl. Soc., 16, 191-192 (1973).

[9] BELYTSCHKO, T. B., KENNEDY, J. M., and MARCHERTAS, A. H., "Dynamic Response of Fast-Reactor Core Subassemblies," Nuclear Engineering and Design, 28, 31-41, (1974).

[10] DEAN, J. S., "Approximate Calculations for the Radial Expansion of Thin Tubes Used in Pressure Transducers," J. of Strain Analysis, 8(4), 264-266 (1973).

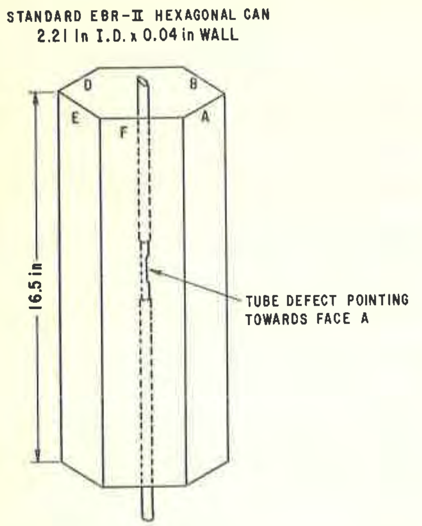

Figure 1 Fuel-pin Rupture Tube in Hexagonal Wrapper Subassembly Test Rig

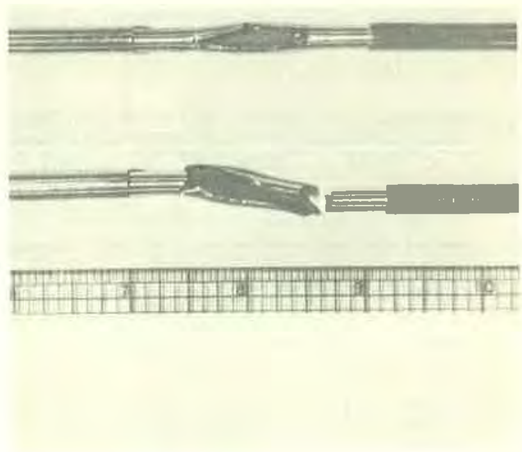

Figure 2 Typical Ruptured Tubes

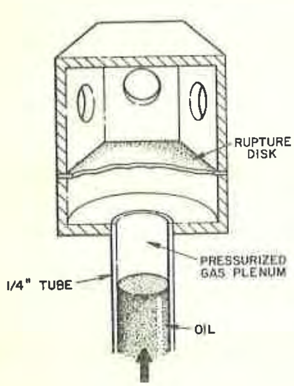

Figure 3

Symmetrical Orifice Configuration for Simulated Experimental Pressure-pulse Source

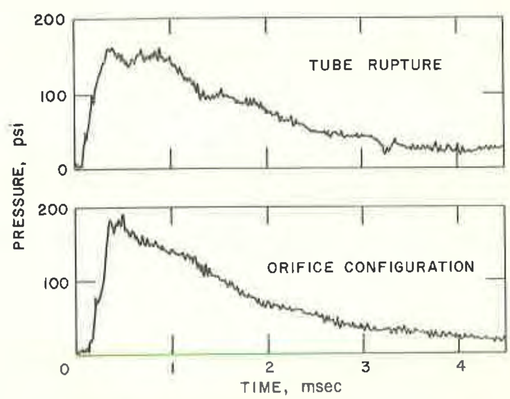

Figure 4

Comparison of Test Pressure Traces for the Symmetrical Orifice Arrangement and the Single Tube Rupture

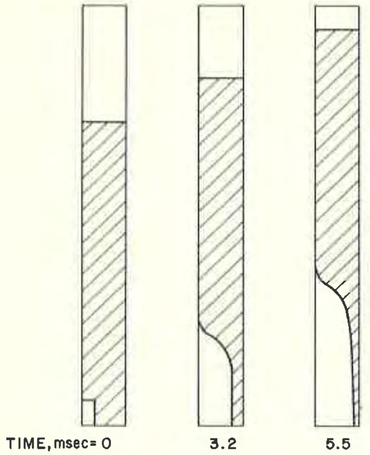

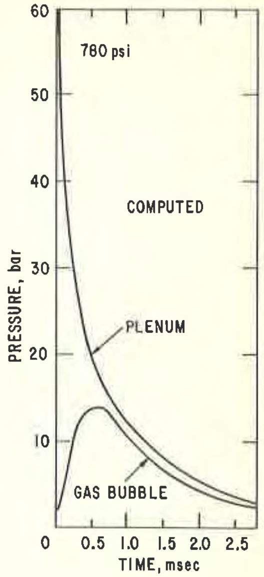

Figure 5

Computed Bubble Growth and Rise of Free Surface

Figure 6

Computed Pressure Histories Inside the Ruptured Tube (Plenum) and in the Discharge Gas Bubble

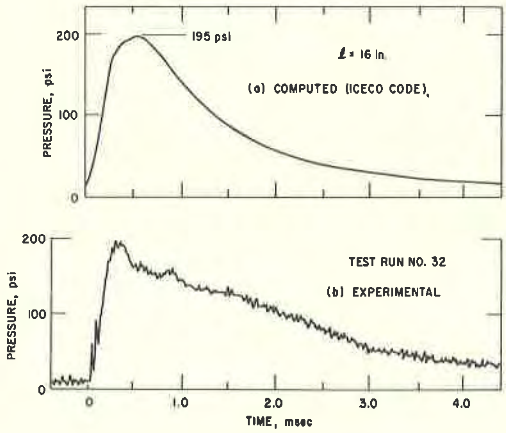

Figure 7 Comparison of Computed and Experimental Pressure Traces at Wall Opposite Orifices

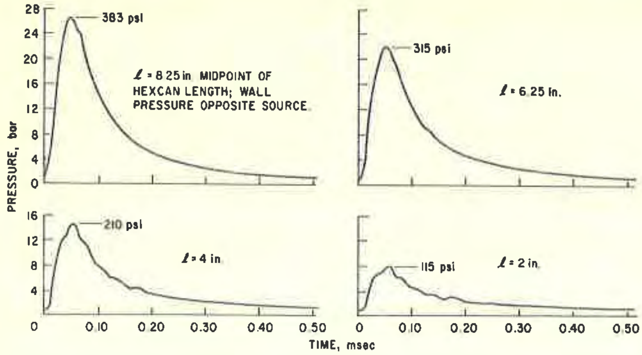

Figure 8 Computed Pressure Traces at Stations Distant ℓ from Top of Hexcan (Source Pressure: 2000 psi; Peak Gas-Bubble Pressure: 410 psi)

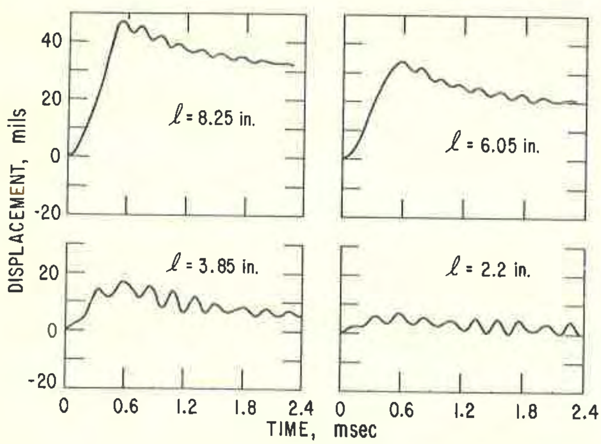

Figure 9 Computed Hexcan Displacement Histories at Fixed Stations for the Pressure Loading Shown in Fig. 8.

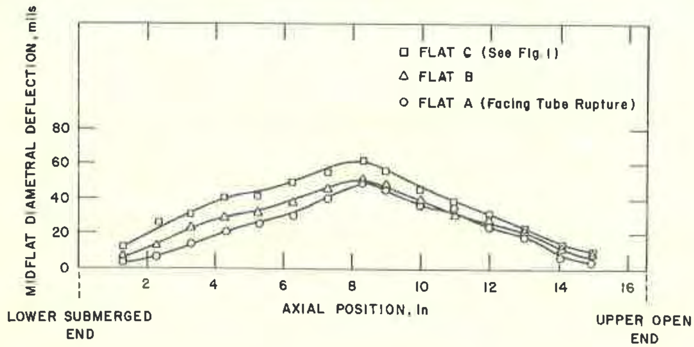

Figure 10 Permanent Increase in Flat-to-Flat Diameter Along Axial Length of Hexcan. (Fuel-pin Rupture Pressure: 2000 psi; Plenum Gas Volume: 22 cc)

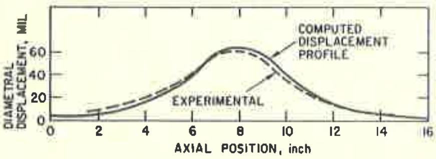

Figure 11
Comparison of the Computed Permanent Displacement Profile Along the Midflat with the Experimental Values

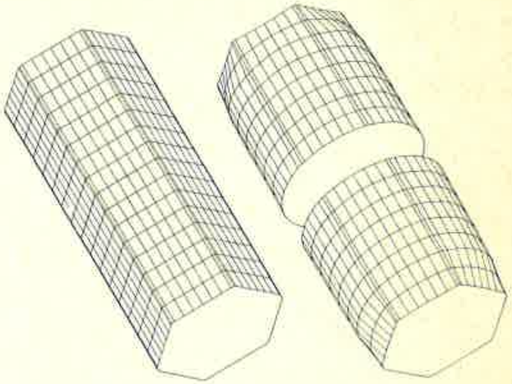

Figure 13
Finite-element Computational Grid for the Annealed Type 316 Stainless Steel Hexcan: (a) Initial Configuration; (b) Configuration at 3000 psi Pressurization.

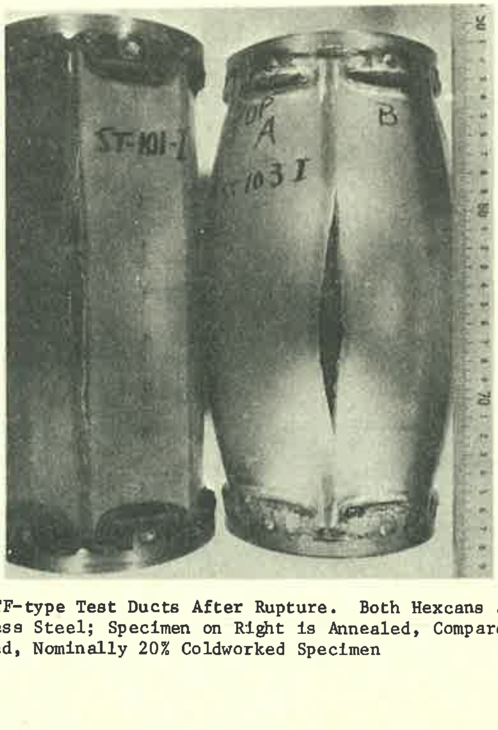

Figure 12 The FFTF-type Test Ducts After Rupture. Both Hexcans are Type 316 Stainless Steel; Specimen on Right is Annealed, Compared with As-Received, Nominally 20% Coldworked Specimen

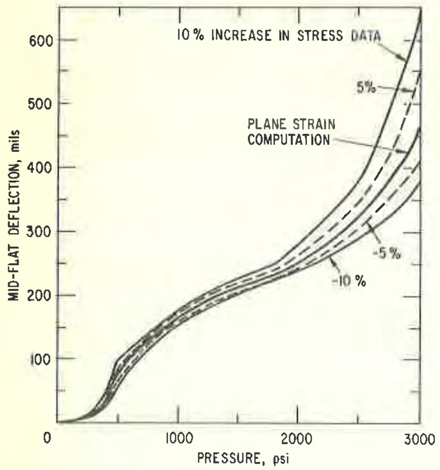

Figure 14
Two-dimensional Computations of Plane Strain for Maximum Midflat Deflections Under Hydrostatic Loading, Showing Sensitivity to Stressstrain Data

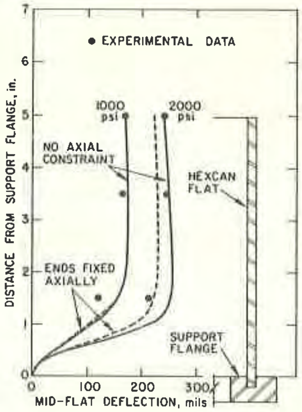

Figure 15
Computed (SADCAT) Deflections in End Region Showing Effects of Axial End Constraints

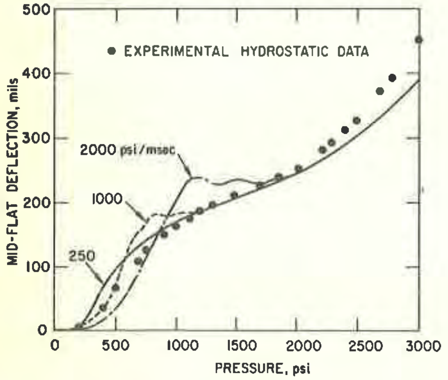

Figure 16
Effects of Loading Rate Upon Midflat Deflections as Shown by SADCAT Computations

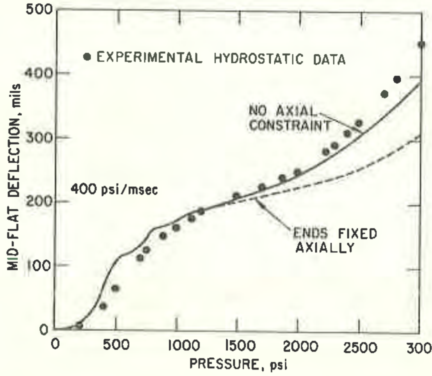

Figure 17
Effects of End Constraints Upon Midflat Deflections as Shown by SADCAT Computations